Diffraction at HERA

M. Kapishin (on behalf of the H1 and ZEUS Collaborations)

JINR, Joliot Curie 6, 141980 Dubna, Russia
kapishin@sunse.jinr.ru

Abstract

Recent experimental results on the inclusive diffractive cross section and diffractive dijet production in deep-inelastic scattering, obtained by the H1 and ZEUS experiments at HERA, are presented. The latest results on the exclusive diffractive production of vector mesons and Odderon searches are also covered. QCD based theoretical models for diffractive ep scattering are discussed and compared with the experimental data.

1 Introduction

The observation of events with a large rapidity gap in the hadronic final state at HERA [1] which are attributed to diffractive dissociation of virtual photons led to a renewed interest in the study of the underlying dynamics of diffraction. Diffractive scattering is governed by the exchange of the Pomeron ($\mathbb{P}$), an object carrying vacuum quantum numbers.

Pomeron exchange was introduced in the Regge theory [2] to describe the high energy behavior of total hadron cross sections [3], which are related to elastic scattering through the optical theorem.

In perturbative QCD (pDCD) the vacuum exchange is modeled as a color singlet exchange of gluons [4] that develops into a gluon ladder between the photon and the proton. pQCD calculations are possible for diffractive processes where a hard scale is present: production of high mass quarks, high momentum jets, processes with high virtuality Q^2 or squared four-momentum transfer t.

At HERA, by changing Q^2 and t, it is possible to vary the resolution with which the Pomeron structure is probed in diffractive interactions, and to study its partonic content. HERA is thus an unique facility to study the transition from soft to hard interactions.

2 Inclusive diffraction

2.1 Kinematics and selection of diffractive ep scattering

The diffractive process $ep \to e'XY$ is illustrated in Fig. 1. The photon with virtuality Q^2 interacts with proton to produce two final state systems X and Y which are separated by a large

rapidity gap if their invariant masses are small.

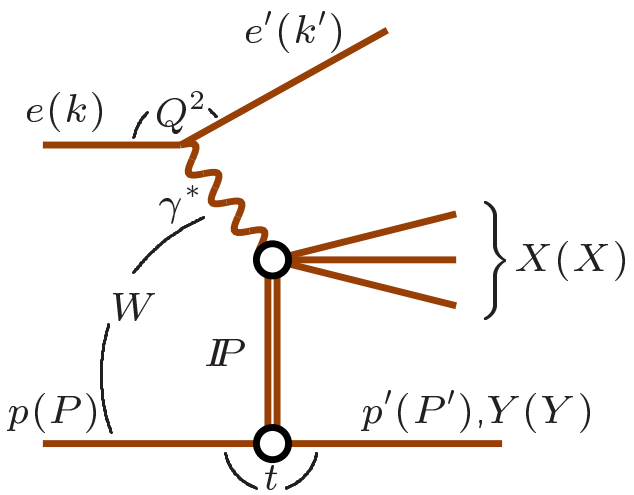

Figure 1: Diagram of diffractive deep inelastic ep scattering

Diffractive deep-inelastic scattering process can be expressed in terms of the variables Q^2, t, Bjorken x and the invariant masses of the $\gamma^* p$, X and Y systems (W, M_X and M_Y, respectively). In addition, the following variables are introduced:

$$x_{I\!P} = \frac{q \cdot (p - p')}{q \cdot p} \simeq \frac{Q^2 + M_X^2}{Q^2 + W^2} \quad , \quad \beta = \frac{Q^2}{2q \cdot (p - p')} \simeq \frac{Q^2}{Q^2 + M_X^2} \quad , \quad x = \beta \cdot x_{I\!P},$$

where q, p and p' are the 4-vectors of the virtual photon, incoming proton and scattered proton, respectively. In the proton infinite momentum frame, $x_{I\!P}$ is the fraction of the beam proton momentum carried by the Pomeron, β is the fraction of the Pomeron momentum carried by struck parton.

Experimentally, diffractive events can be selected by the direct observation of a large rapidity gap in the detector [5]. Kinematics imply that a gap in rapidity is created between the system X and the scattered proton when $x_{I\!P} \ll 1$, i.e. $M_X \ll W$. Another method exploits the fact that diffractive interactions are characterized by a non-exponentially suppressed rapidity gap [6]. Diffractive processes are selected as an excess of events over the exponential fall-off of the $\ln M_X^2$ distribution of non-diffractive events. These methods yield a mixture of events containing an intact final state proton and events where the proton dissociates, since a low-mass system Y cannot be detected.

Diffractive events can also be detected using leading proton spectrometers (LPS) which measure the momentum of the scattered proton [7]. This provides a clean measurement of elastic diffraction without proton dissociation background and allows the measurement of the t distribution. However the geometrical acceptance of these detectors is low.

2.2 Models of diffractive deep-inelastic scattering

In analogy with non-diffractive DIS, the inclusive diffractive cross section is expressed in the form of a structure function dependent on four variables:

$$\frac{\mathrm{d}^3\sigma(ep \to epX)}{\mathrm{d}\beta \mathrm{d}Q^2 \mathrm{d}x_{\mathbb{P}} \mathrm{d}t} = \frac{4\pi\alpha^2}{\beta Q^4}(1 - y + \frac{y^2}{2})\mathrm{F}_2^{\mathrm{D}(4)}(\beta, Q^2, x_{\mathbb{P}}, t)$$

where the contribution of the longitudinal structure function F_L was neglected.

It has been proved that F_2^D factorize 7) actresses into long and short-distance contributions in analogy with the inclusive F_2 (QCD factorizing), i.e.

$$F_2^D \sim f^D(\beta, Q^2, x_{\mathbb{P}}, t) \otimes \hat{\sigma}(\beta, Q^2)$$

where $\hat{\sigma}$ are cross sections for pQCD hard scattering and f^D are diffractive parton densities, which obey the DGLAP evolution equations for fixed $x_{\mathbb{P}}$ and t, and are universal [8]. If for all relevant f^D the $x_{\mathbb{P}}$ and t dependences decouple from the β and Q^2 dependences, it is known as Regge factorisation or "resolved Pomeron" model [9] (see Fig. 2):

$$F_2^D(\beta, Q^2, x_{\mathbb{P}}, t) = \Phi(x_{\mathbb{P}}, t) \cdot F_2^{\mathbb{P}}(\beta, Q^2)$$

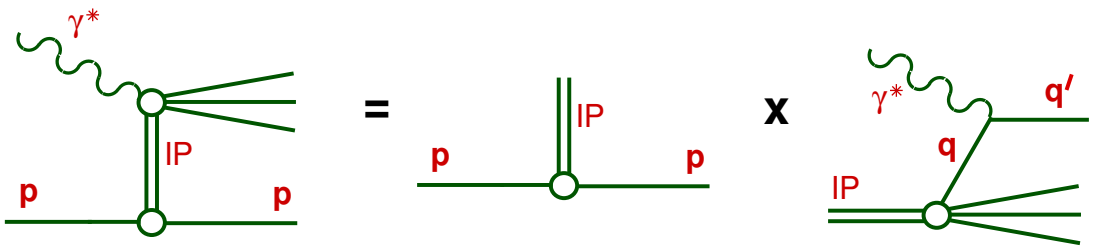

Figure 2: Diagram of diffractive process in the "resolved Pomeron" model.

In this case $\Phi(x_{\mathbb{P}}, t)$ can be interpreted as the flux of the Pomeron, and $F_2^{\mathbb{P}}$ as the structure function of the Pomeron. The flux factor describes the long-distance physics at the proton vertex, while the structure function depends on the exchanged parton densities and the short-distance physics at the photon vertex. Regge theory predicts the following form for the flux factor:

$$\Phi(x_{\mathbb{P}}, t) = e^{B_{\mathbb{P}} t} \cdot (\frac{1}{x_{\mathbb{P}}})^{2\alpha_{\mathbb{P}}(t)-1}$$

where $\alpha_{\mathbb{P}}(t) = \alpha_{\mathbb{P}}(0) + \alpha'_{\mathbb{P}} t$ describes the Pomeron trajectory.

In y's 8) factored dipole models the virtual photon is considered to fluctuate into $q\overline{q}$ or $q\overline{q}g$ states described by dipole wave functions [10]. In the proton rest frame and at low Bjorken x the fluctuation happens long before the interaction with the proton. The diffractive $\gamma^* p$ cross section

is factorized into the square of the effective dipole wave function and the cross section for the diffractive scattering of the dipole off the proton. The dipole cross section can be calculated in pQCD for relatively high values of Q^2. The β dependence of the diffractive structure function is fixed by three contributions, corresponding to $q\overline{q}$ production by longitudinally and transversely polarized photons and $q\overline{q}g$ production by transversely polarized photons. The $q\overline{q}g$ configuration dominates at low β, while the longitudinal $q\overline{q}$ is of higher twist nature and dominates at high β. The medium β region is populated dominantly by $q\overline{q}$ final states originating from transversely polarized photons.

There are several color dipole models which differ in the way they treat the actual dipole-proton interaction.

In the "two gluon exchange model" [12] the photon fluctuations scatter elastically off the proton through the exchange of two gluons in a net color-singlet configuration. The dipole-proton cross section is proportional to the square of the gluon density inside the proton. The model requires high transverse momentum of all outgoing partons (including gluons with $p_T^g > p_T^q$), thus it is particularly suited for diffractive high E_T jet production. In order to avoid the contribution of the valence quarks in the proton and the secondary Reggeon exchanges, the model is restricted to the range $x_{\mathbb{P}} < 0.01$.

In the "saturation model" [13] the dipole cross section is parametrized as a function of the transverse size of the dipole (r) and grows from the color transparency regime at small radii (large Q^2) and saturates at a constant value at large radii.

Saturation at low x is explicitly built-in through an x-dependent effective saturation radius R_0.

$$\hat{\sigma}(x, r^2) = \sigma_0[1 - \exp(-\frac{r^2}{4R_0^2(x)})] \qquad R_0(x) = \frac{1}{\mathrm{GeV}}(\frac{x}{x_0})^{\lambda/2}$$

After a fit of the dipole cross section to the inclusive $F_2(x, Q^2)$, the model predicts the diffractive structure function including the small Q^2 region where pQCD calculations can not be applied. The model predicts that the ratio of the diffractive to the inclusive cross section is approximately constant as a function of W.

In the "semi-classical model" [14] the photon dipole fluctuation interacts non-perturbatively with the average color field of the proton. Diffraction occurs if the emerging partonic state is a color singlet. Partonic distributions are calculated at some low scale Q_0^2 and follow the DGLAP evolution to predict diffractive and inclusive structure functions. The diffractive gluon density is predicted to be much higher than the diffractive quark density.

3 F_2^D measurements

The $x_{\mathbb{P}}, \beta$ and Q^2 dependence of $F_2^{D(3)}$ is studied in a new high precision measurement of the H1 experiment [16]. The data were integrated over the measured t-range ($|t| < 1\mathrm{GeV}^2$).

The measured structure function $x_{\mathbb{P}}F_2^{D(3)}(\beta, Q^2, x_{\mathbb{P}})$, shown in Fig. 3 and 4 for fixed $x_{\mathbb{P}}$ values, indicates a rising scaling violation with $\ln Q^2$, persisting up to relatively large value of $\beta \sim 0.65$. When compared with the inclusive F_2 at fixed $x = \beta \cdot x_{\mathbb{P}}$, the Q^2 dependences of F_2 and F_2^D are similar for $\beta \lesssim 0.65$ for the diffractive case, indicating that similar dynamics work in two processes. At the highest β, the F_2^D scaling violation becomes negative and there is a clear difference between the inclusive and diffractive Q^2 dependences at the same x. In the high β region, higher twist contributions such as vector meson production could play a major role in the diffractive cross section [13]. A QCD fit was performed in which the parton densities in the Pomeron were evolved according to the leading order DGLAP equations. The result of the fit is compared with the data in Fig. 4. The logarithmic scaling violation is described by the fit, which predicts that partonic momentum distribution of the Pomeron dominated by gluons.

In the Regge approach, the $x_{\mathbb{P}}$ dependence is assumed to factorize from the (β, Q^2) dependence:

$$x_{\mathbb{P}}F_2^{D(3)} = A(\beta, Q^2)x_{\mathbb{P}}^{2-2\alpha_{\mathbb{P}}(\overline{t})}$$

where $\alpha_{\mathbb{P}}(t)$ is the effective Pomeron trajectory at the mean t value of the measurement. No significant variation of the effective $\alpha_{\mathbb{P}}(0)$ intercept with β or Q^2 was found. The measured $\alpha_{\mathbb{P}}(0)$ is compared in Fig 5 with previous inclusive and diffractive DIS and photo-production measurements.

Simple Regge predictions for the inclusive F_2 lead at fixed Q^2 and low x to $F_2(x, Q^2) \propto x^{1-\alpha_{\mathbb{P}}(Q^2)}$. The effective intercepts describing the inclusive and diffractive energy dependences become different at large Q^2. Regge phenomenology predicts a factor of two faster growth of the diffractive in comparison with the inclusive cross section with decreasing x (increasing W). The H1 and ZEUS experiments measured that the ratio of diffractive to inclusive cross sections in DIS is relatively flat as a function of W when M_x, β and Q^2 are fixed [6, 16]. Regge predictions for the ratio of the diffractive to inclusive cross sections hold in the range $Q^2 < 1\mathrm{GeV}^2$.

ZEUS diffractive data presented in Fig. 6 are well described by the "saturation model" [13] in the range $Q^2 > 4\mathrm{GeV}^2$ and show the dominance of the $q\overline{q}g$ contribution at large M_X. Still, the model is not able to reproduce the data at $Q^2 < 1\mathrm{GeV}^2$. The "saturation" and "semi-classical" models [13, 14] reproduce general features of the H1 $F_2^{D(3)}$ data [16], but lie above the data where β and Q^2 are both small.

The H1 and ZEUS experiments measured the t-slope b of $\mathrm{d}\sigma/\mathrm{d}t \propto \exp(bt)$ using their leading proton spectrometers (LPS) [17, 18]. The slope b is a measure of the interaction radius $R(b \sim R^2/4)$ and is expected to rise with decreasing $x_{\mathbb{P}}$ according to the Regge model prediction: $b \simeq b_0 + 2\alpha' \ln(1/x_{\mathbb{P}})$ ("shrinkage" effect). QCD predicts a much reduced "shrinkage" effect for the Pomeron. The results of the measurements shown in Fig. 7 are not conclusive yet at low $x_{\mathbb{P}} < 10^{-2}$.

The diffractive structure function $F_2^D(3)$ measured in the H1 and ZEUS experiments by the LPS method [17, 18] is compatible with $F_2^{D(3)}$ measured by the large rapidity gap method [16]. This is an indication that the proton dissociation contribution to the latter measurement is small.

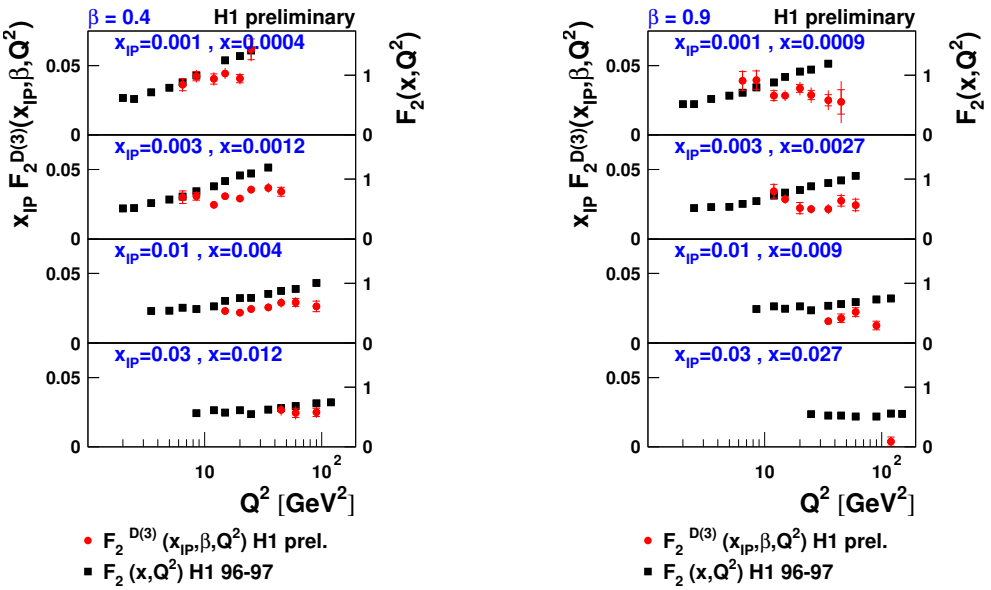

Figure 3: The H1 measured diffractive structure function $x_{\mathbb{P}}F_2^{D(3)}(\beta, Q^2, x_{\mathbb{P}})$ plotted as a function of Q^2 for two fixed values of $\beta = 0.4$ and $\beta = 0.9$ and for fixed $x_{\mathbb{P}}$. Also shown are $F_2(x, Q^2)$ data from [19], where $x = x_{\mathbb{P}}\beta$

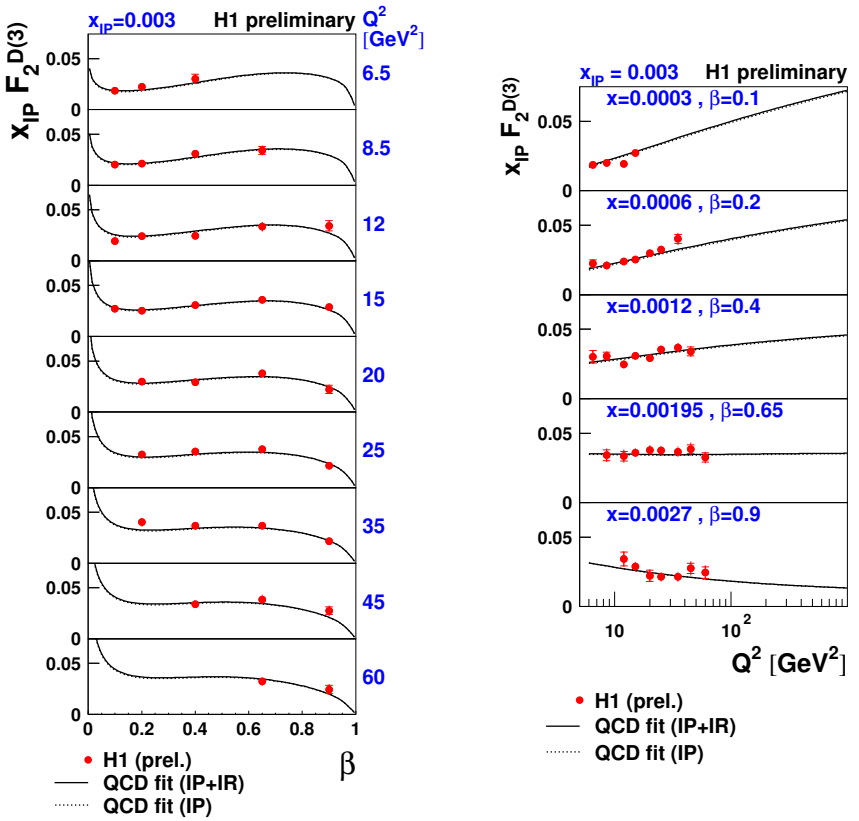

Figure 4: The H1 measured diffractive structure function $x_{\mathbb{P}}F_2^{D(3)}(\beta, Q^2, x_{\mathbb{P}})$ plotted as a function of β and as a function of Q^2 at fixed value of $x_{\mathbb{P}} = 0.003$. Also shown is the result of a QCD fit to the data.

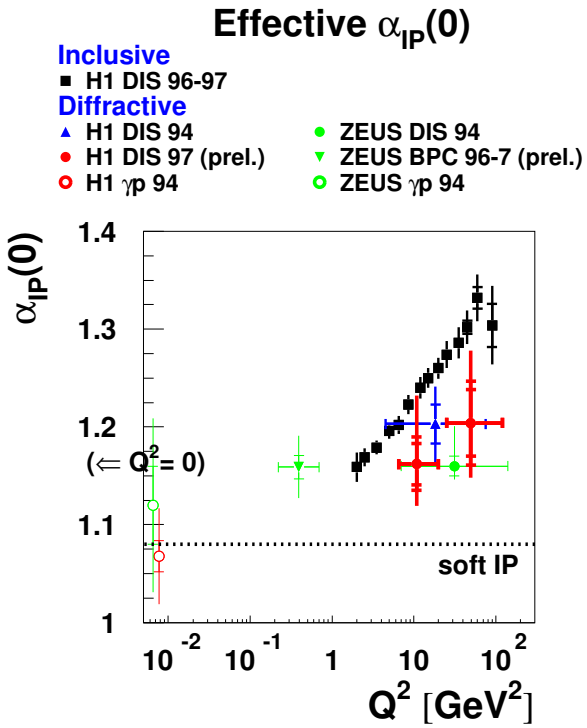

Figure 5: The effective Pomeron intercept $\alpha_{\mathbb{P}}(0)$ measured in inclusive and diffractive DIS and photoproduction as a function of Q^2

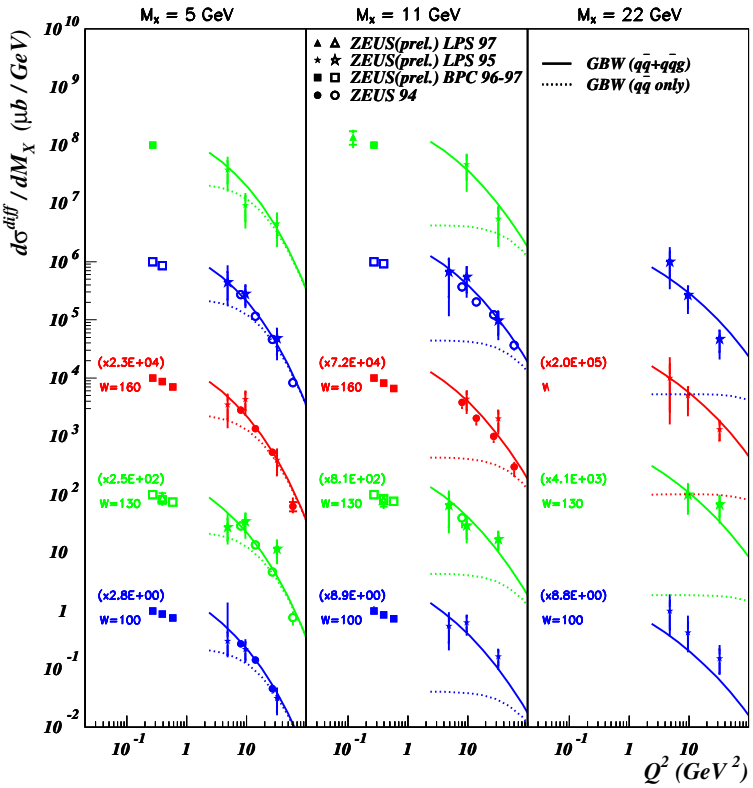

Figure 6: The ZEUS measured diffractive differential cross section $\mathrm{d}\sigma/\mathrm{d}M_X$ plotted as a function of Q^2, compared with the "saturation" model [13]

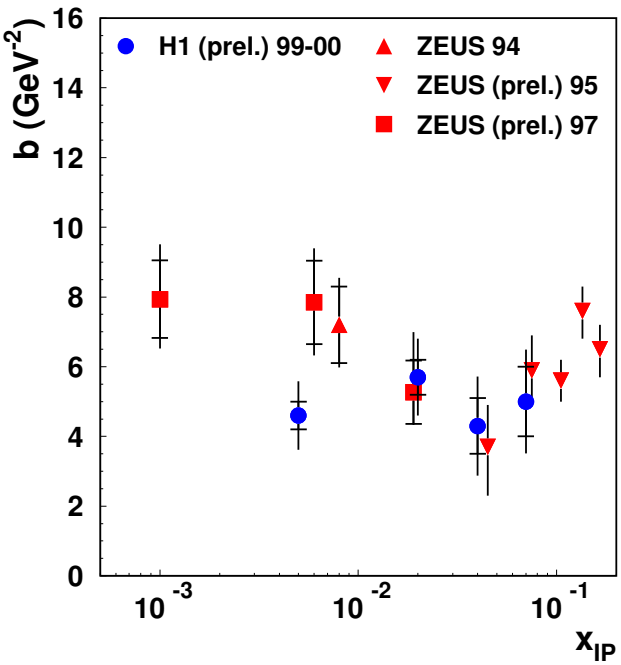

Figure 7: The slope parameter b of the differential cross section $\mathrm{d}\sigma/\mathrm{d}t$ as a function of $x_{\mathbb{P}}$. Results obtained with the H1 and ZEUS LPS are shown.

4 Diffractive jet production

According to the QCD factorisation theorem [8], parton distributions extracted from the QCD fits to inclusive diffraction can be exported to hadronic final states in DIS for the same $x_{\mathbb{P}}$ and t. Of particular interest is the measurement of diffractive dijet production, since the implied boson gluon fusion process $\gamma^* g \to q\overline{q}$ provides a direct probe of the gluon content of the Pomeron.

In Fig. 8 the quantity $z_{\mathbb{P}}^{jets} = (Q^2 + M_{12}^2)/(Q^2 + M_X^2)$, representing the fraction of the hadronic energy in the final state contained in two jets with the invariant mass M_{12}, is compared with the prediction from the "resolved Pomeron" model [9] based on different sets of Pomeron gluon distributions obtained from the leading order DGLAP analysis of $F_2^{D(3)}$ by H1 [5] and others [15].

The data favor the Pomeron dominated by gluons with a gluon momentum distribution that is relatively flat in $z_{\mathbb{P}}^{jets}$. For diffractive scattered $q\overline{q}$ photon fluctuations, a distribution peaked at $z_{\mathbb{P}} \sim 1$ is expected. The low values of $z_{\mathbb{P}}$ correspond to dominance of $q\overline{q}g$ over $q\overline{q}$ scattering. The $x_{\mathbb{P}}$ and β distributions of the dijet cross section are also in agreement with the "resolved Pomeron" model with the Pomeron intercept $\alpha_{\mathbb{P}}(0)$ extracted from inclusive $F_2^{D(3)}$ [5].

5 Exclusive diffraction

5.1 Search for the Odderon in exclusive π^0, f_2, a_2 photo-production

The Odderon is a possible partner of the Pomeron trajectory with an intercept $\alpha_{\mathbb{O}} \approx 1$ and $C = P = -1$ [20].

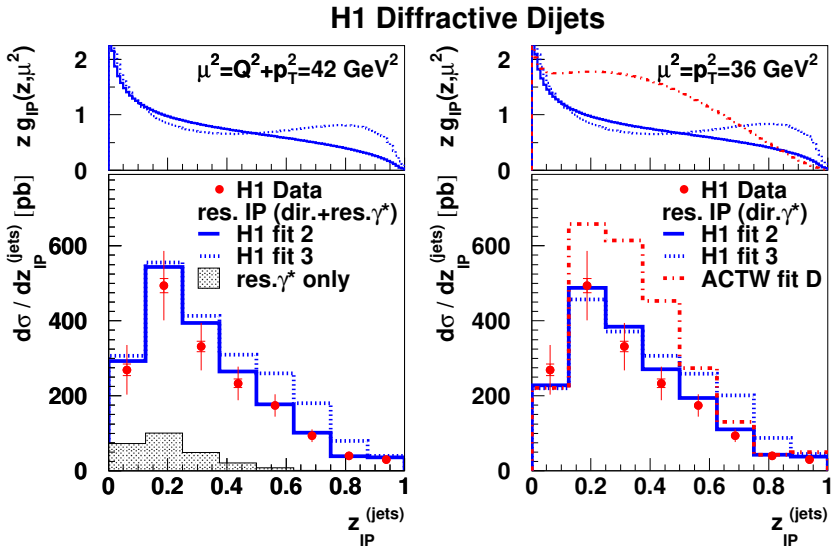

Figure 8: The diffractive dijet cross section as a function of $z_{\mathbb{P}}$ compared with predictions of the "resolved Pomeron" model based on the QCD fits [5, 15].

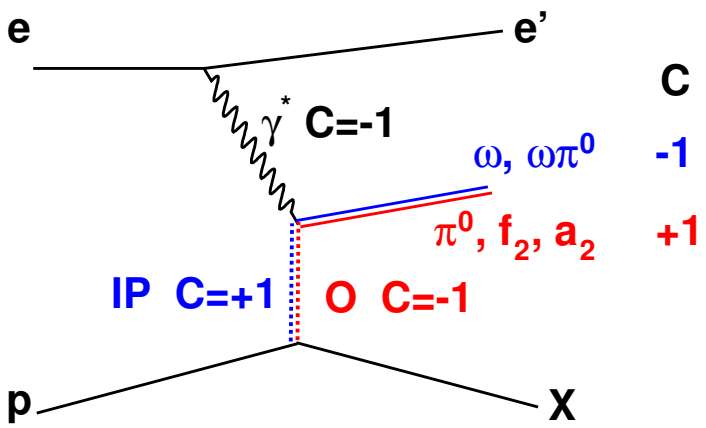

Figure 9: Diagram of exclusive π^0, f_2, a_2 photo-production via Odderon-photon fusion.

In the Regge picture the presence of the Odderon amplitude would lead to a difference in the total hadron-hadron (hh) and hadron-antihadron ($h\overline{h}$) cross sections at high energies. Global fits of the available hh and $h\overline{h}$ data show no evidence for the Odderon and seem to establish the conventional Regge picture, with high energy scattering dominated by exchange of the Pomeron ($C = P = +1$) with the contribution of other Reggeon exchanges at lower energies ($\alpha_{\mathbb{R}} \approx 0.5$) [3]. In the QCD picture the Odderon exchange is interpreted as exchange of three gluons. Exclusive photo-production and electroproduction-production of pseudo-scalar (π^0) and tensor mesons (f_2, a_2) via Odderon-photon fusion are reactions where Pomeron exchange cannot contribute, and their measurement would therefore be a clear proof of the existence of the Odderon (Fig. 9).

Such reactions are accessible at the ep collider HERA, but no signal was found in multi-

photon final states. The measured upper limits of the cross sections,

$$\sigma(\gamma p \xrightarrow{\mathbb{O}} \pi^0 N^*) < 39 \text{ nb},$$
$$\sigma(\gamma p \xrightarrow{\mathbb{O}} f_2(1270) N^*) < 16 \text{ nb},$$
$$\sigma(\gamma p \xrightarrow{\mathbb{O}} a_2(1320) N^*) < 96 \text{ nb},$$

all at 95% CL, are below the predictions of a model based on non-perturbative QCD [21].

5.2 Exclusive vector meson production

Diffractive vector meson production follows a description similar to elastic hadron-hadron scattering, if no hard scale is present.

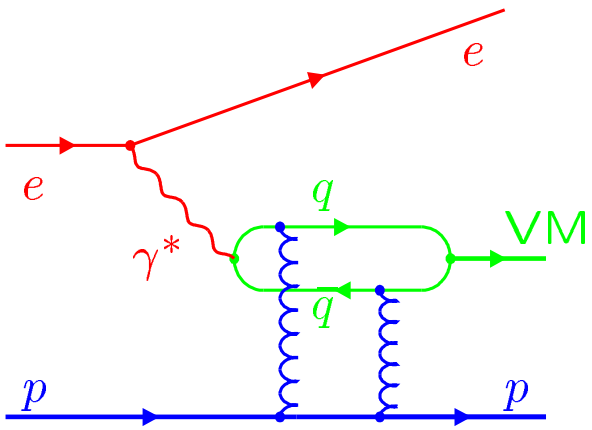

Figure 10: Diagram of diffractive vector meson production in ep scattering.

However, when the scales $Q^2, |t|$ or the squared vector meson mass M_V^2 become large, deviations from the soft Pomeron behavior become clear and a pQCD description is applicable. In the lowest order pQCD, the process of diffractive vector meson production in ep scattering is viewed as a fluctuation of the virtual photon into $q\overline{q}$ pair which subsequently interacts with the proton via the exchange of two gluons in a color singlet state and later evolves into a real vector meson (see Fig. 10). Models of hard vector meson production, that predict the cross section to be proportional to the square of the gluon distribution of the proton [22], give good descriptions of the data.

In presence of a "hard" scale, pQCD predicts a steep rise of the cross section with $W_{\gamma p}$. It is confirmed in elastic J/ψ photo-production at low $|t|$, where the exchange of the soft Pomeron trajectory $\alpha_{\mathbb{P}}(t) = 1.08 + 0.25t$ [3] does not describe the data measured by the ZEUS experiment ($\alpha_{\mathbb{P}} \simeq 1.193 + 0.105t$) [24] and the H1 experiment ($\alpha_{\mathbb{P}} \simeq 1.27 + 0.08t$) [23].

Recently, new data at large values of $|t|$ have become available to test the applicability of the scale variable $|t|$ for pDCQ calculations. At large $|t|$, proton dissociative J/ψ photo-production

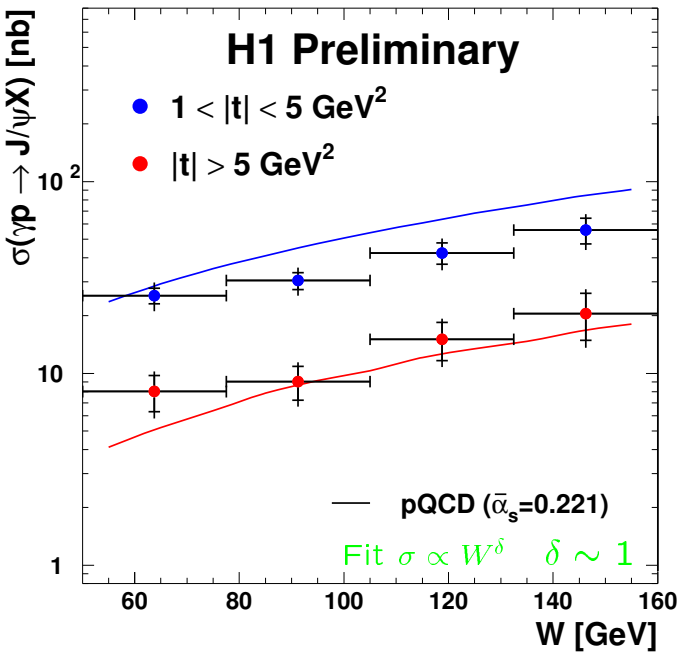

Figure 11: J/ψ photo-production proton dissociation cross section at large $|t|$ as a function of W. Predictions of the BFKL model are also shown.

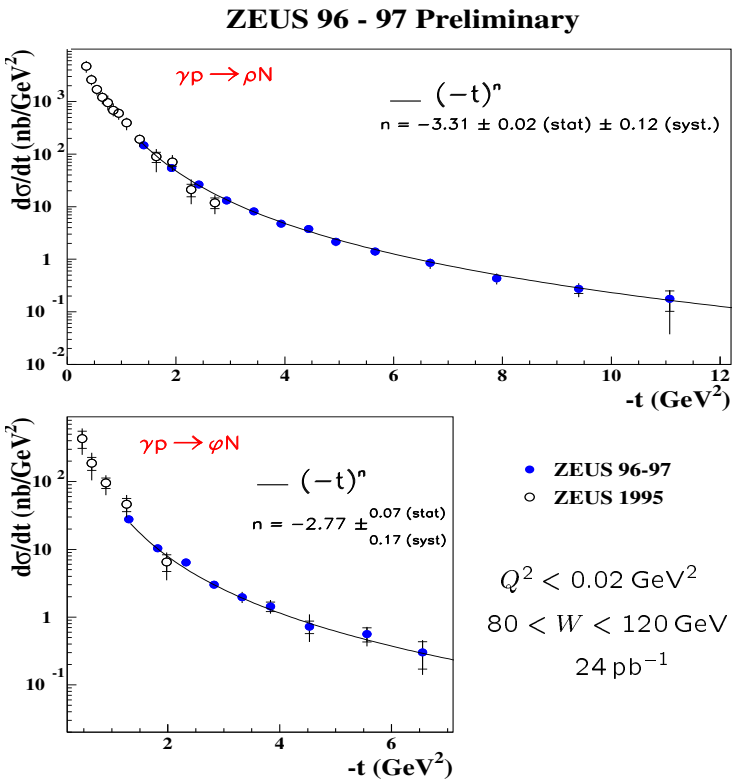

Figure 12: ρ and ϕ meson differential photo-production cross section as a function of t. The results of the fit by the power law dependence $(-t)^n$ are also shown.

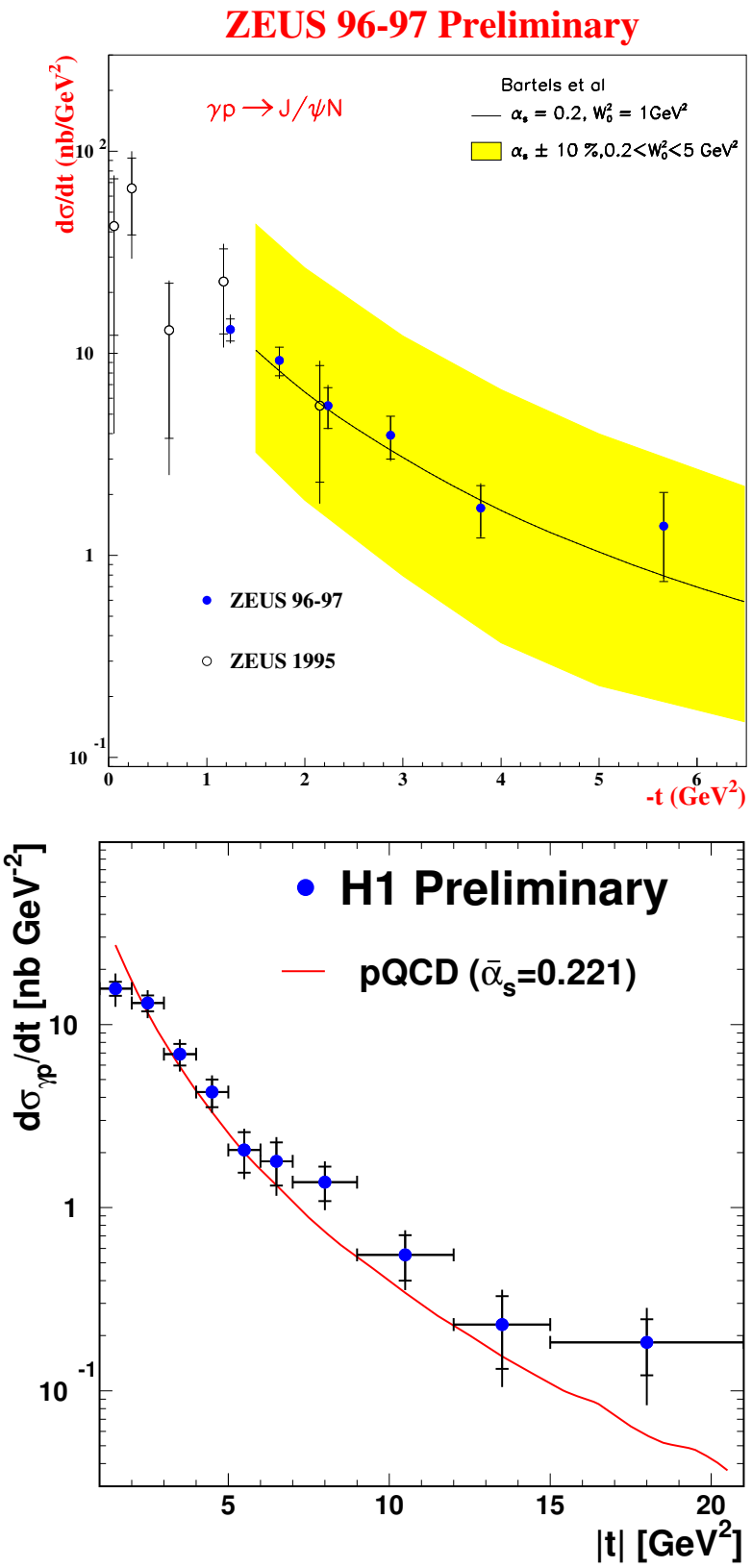

Figure 13: J/ψ proton dissociation photo-production cross sections as a function of $|t|$. Predictions of the BFKL model are also shown.

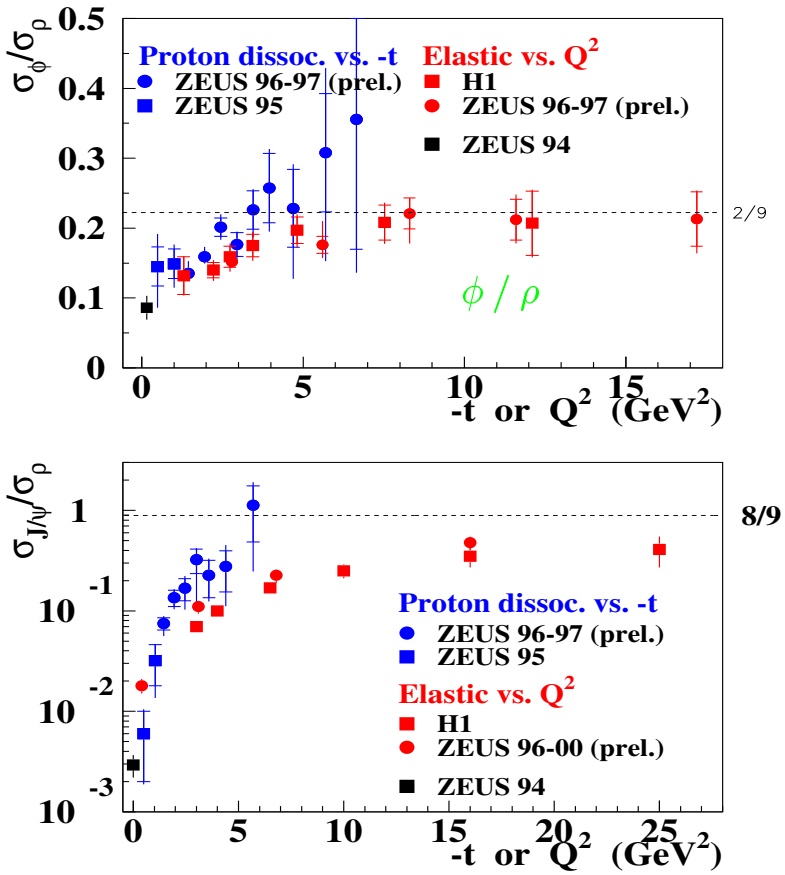

Figure 14: The cross section ratios σ_ϕ/σ_ρ and $\sigma_{J/\psi}/\sigma_\rho$ as functions of t and Q^2. Predictions based on the SU(4) symmetry are also shown.

cross section [25] shows W-dependence similar to elastic J/ψ photo-production and is nicely described by the pQCD model based on the BFKL evolution [22] with an assumption $\overline{\alpha_s} \sim 0.20$ (see Fig. 11).

The t-dependence of the cross section at large values of $|t|$ in pQCD is expected to follow a power law form $|t|^n$ [26], that is slower than the exponential t-dependence measured at low $|t|$ [23, 24]. The ZEUS experiment measured ρ and ϕ photo-production cross sections with proton dissociation at $|t| > 1\mathrm{GeV}^2$ [27]. The data reveal a power law $|t|$-behavior with $n \simeq 3$ (Fig. 12). Proton dissociative J/ψ photo-production cross sections at large $|t|$, measured by the H1 and ZEUS experiments [25, 27], are shown in (Fig. 13). The cross sections are described by the BFKL model [22] taking into account the model uncertainty. Compared to light vector mesons, the $|t|$-dependence is even flatter ($|t|^n$ with $n \simeq 1.7$).

Following the predictions for the coupling of the photon to a vector meson, based on a simple charge counting of the quark content of the vector meson, the cross section ratios $\rho : \phi : J/\psi$ should be $9 : 2 : 8$. The cross section ratios σ_ϕ/σ_ρ and $\sigma_{J/\psi}/\sigma_\rho$ are shown in Fig. 14 as a function of the Q^2 and $|t|$ variables. The Q^2 dependence is obtained from elastic data at low $|t|$. While the ratio σ_ϕ/σ_ρ reaches the expected value 2/9 at high Q^2, the ratio $\sigma_{J/\psi}/\sigma_\rho$ is significantly lower than the naive expectation of 8/9 even at high Q^2. The proton dissociation

data, plotted as a function of $|t|$ in the same figures, also rise steeply with $|t|$, indicating that $|t|$ is indeed a "hard" scale variable. However quantitatively, the $|t|$-behavior is different than that with Q^2.

6 Summary

Recent results on diffraction at HERA have been reviewed. New inclusive and exclusive measurements cover a wide kinematic range. The precision of data has been increased significantly.

The inclusive diffractive data show that at large Q^2 the effective Pomeron intercept becomes larger than that of the soft Pomeron describing high energy hadron-hadron scattering. This motivates a perturbative QCD approach to be applied. The "resolved Pomeron" model and models based on the color dipole approach give reasonable descriptions of inclusive and dijet diffraction. The "saturation model" describes transition from the hard to the soft region at low Q^2. A QCD-motivated fit of the diffractive structure function $F_2^{D(3)}$ that is based on the "resolved Pomeron" approach and the DGLAP evolution equations requires the Pomeron structure to be dominated by gluons carrying a large fraction of the exchanged momentum. This conclusion is confirmed through the measurement of final state observables such as the diffractive dijet cross section.

Scaling violations of F_2 and F_2^D are similar except in the range of large β (small M_X), where higher-twist contributions play a role in the diffractive processes. The $\gamma^* p$ cms energy dependences of the diffractive and total cross sections follow Regge predictions at low Q^2 and become similar at large Q^2. This behavior is predicted by the saturation model.

For the case of exclusive vector meson production in the presence of a hard scale, QCD models, which describe the process as a fluctuation of the photon into $q\overline{q}$ pair and a subsequent exchange of two gluons with the proton, successfully reproduce the steeper W-dependence and weaker t-dependence of the cross section than expected in the Regge approach. Vector meson production ratios reach the SU(4) predictions at large $|t|$ indicating that t can be considered as a "hard" scale variable. But quantitatively the $|t|$ behavior is different from that with Q^2.

No Odderon signal was found in exclusive pseudo-scalar and tensor meson production at HERA. The upper limits of the cross sections are below the predictions of a non-perturbative Odderon model.

References

[1] ZEUS Collaboration, M. Derrick *et al.* Phys. Lett. **B315** (1993) 481
H1 Collaboration, T. Ahmed *et al.* Phys. Lett. **B429** (1994) 477

[2] K. Goulianos, Phys. Rev. **101** (1983) 169

[3] A. Donnachie, P. Landshoff, Phys. Lett. **B296** (1992) 227

[4] F. Low, Phys. Rev. **D12** (1975) 163
S. Nussinov, Phys. Rev. Lett. **34** (1975) 1286

[5] H1 Collaboration, C. Adloff *et al.* Z. Phys. **C76** (1997) 613

[6] ZEUS Collaboration, J. Breitweg *et al.*, Eur. Phys. J. **C6** (1999) 43

[7] ZEUS Collaboration, J. Breitweg *et al.*, Eur. Phys. J. **C 1** (1998) 81

[8] J.C. Collins, Phys. Rev. **D 57** (1998) 3051; **D 61** (2000) 019902

[9] G. Ingelman and P.E. Schlein, Phys. Lett. **B 152** (1985) 256

[10] For a review, see M.F. McDermott, DESY 00-126 (2000)

[11] J.Bartels, J.Ellis, H. Kowalski and M. Wuensthoff, Eur. Phys. J. **C7** (1999) 443

[12] J. Bartels, H. Jung and M. Wuensthoff, Eur. Phys. J. **C11** (1999) 111

[13] K. Golec-Biernat and M. Wuesthoff, Phys. Rev. **D 60** (1999) 114023

[14] W. Buchmueller, M.F. McDermott and A. Hebecker, Eur. Phys. **B487** (1997) 283

[15] L. Alvero, J. Collins, J. Terron, J. Whitmore, PSU/TH/177, PSU/TH/200 (1998)

[16] H1 Collaboration, abstract 808, paper submitted to EPS Conference on HEP 2001, Budapest.

[17] H1 Collaboration, abstract 809, paper submitted to EPS Conference on HEP 2001, Budapest.

[18] ZEUS Collaboration, abstract 556, paper submitted to EPS Conference on HEP 2001, Budapest.

[19] H1 Collaboration, C. Adloff *et al.*, DESY-00-181

[20] D. Joynson *et al.*, Nuov.Cim. **30A** (1975) 345

[21] E.R. Berger *et al.*, Eur.Phys.J. **C9** (1999) 491

[22] J.R. Forshaw, M. Ryskin, Z. Phys. **C68** (1995) 137
J. Bartels, H. Lotter, J.R. Forshaw and M. Wuensthoff, Phys. Lett. **B375** (1996) 301

[23] H1 Collaboration, C. Adloff *et al.* Nucl. Phys. **B483** (2000) 23

[24] ZEUS Collaboration, S. Chekanov *et al.* DESY-02-008

[25] H1 Collaboration, abstract 806, paper submitted to EPS Conference on HEP 2001, Budapest.

[26] D.Yu. Ivanov, Phys. Rev. **D53** (1996) 3564

[27] ZEUS Collaboration, J. Breitweg *et al.*, Eur. Phys. J. **C 14** (2000) 213